

MODELLA—A New Physics-Based Compact Model for Lateral p-n-p Transistors

Francis G. O'Hara, Jan J. H. van den Biesen, H. C. de Graaff, W. J. Kloosterman, and J. Barton Foley, *Member, IEEE*

Abstract—A new lateral p-n-p compact model, suitable for computer-aided circuit design purposes, is presented. In this formulation, called MODELLA, the equivalent circuit topology, analytical equations, and model parameters are derived directly from the physics and structure of the lateral p-n-p. MODELLA incorporates current crowding effects, substrate effects, and a bias-dependent output conductance and it uses the approach to lateral p-n-p high injection modeling whereby the main currents and charges are *independently* related to bias-dependent minority-carrier concentrations. Model-specific aspects of the parameter determination strategy are discussed; the Ning-Tang resistance determination method, for example, is shown to be highly suitable for lateral p-n-p devices. The effectiveness of this strategy and the improved performance of this physics-based formulation become evident in comparisons between MODELLA and the standard SPICE Gummel-Poon model using measured device characteristics.

I. INTRODUCTION

IN THE DESIGN of bipolar analog integrated circuits, greater flexibility is often achieved when both n-p-n and p-n-p transistors are incorporated in the circuit design. The type of p-n-p structure used will depend on the performance required, but many present-day bipolar production processes use the conventional lateral p-n-p (see Fig. 1) as the standard p-n-p structure. Because the lateral p-n-p avails itself of the p-type base of the vertical n-p-n transistor to form its emitter and collector regions, no special masks or extra processing steps are required in its manufacture. It is therefore a cost-effective p-n-p implementation, which is relatively simple to manufacture and does not increase process development time. Careful design of these devices can produce transistors with a cutoff frequency up to 100 MHz, and a current gain of 100, while maintaining an Early voltage of 20 V. This is often quite adequate for analog applications such as buffers, current mirrors, level shifting circuitry, current sources, and signal amplifiers.

Manuscript received January 17, 1991; revised April 23, 1992. The review of this paper was arranged by Associate Editor D. D. Tang.

F. G. O'Hara was with Philips Research Laboratories, P.O. Box 80.000, 65 JA Eindhoven, The Netherlands. He is now with Teletronics Pacing Systems, Lane Cove 2066, NSW, Australia.

J. J. H. van den Biesen, H. C. de Graaff, and W. J. Kloosterman are with Philips Research Laboratories, P.O. Box 80.000, 65 JA Eindhoven, The Netherlands.

J. B. Foley is with the Microelectronics Department, University of Dublin (Trinity College), Dublin 2, Ireland.

IEEE Log Number 9202950.

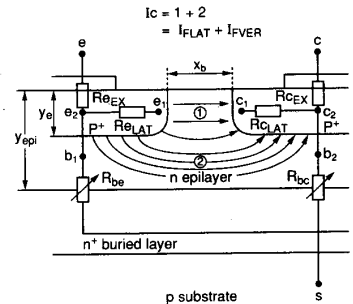


Fig. 1. Schematic cross section of a lateral p-n-p transistor showing the physical origin of the series resistances used in the equivalent circuit of MODELLA. The two-dimensional collector current I_c is shown to consist of two components: 1. I_{flat} —a purely lateral flow originating from the emitter-base sidewall and 2. I_{fver} —a flow along curved trajectories originating from under the emitter. The internal nodes from the circuit diagram in Fig. 2 are indicated.

In spite of their widespread use, however, literature on lateral p-n-p compact modeling for computer-aided circuit design purposes is not very abundant [1]. Today, circuit designers are faced with the following choice of lateral p-n-p compact models:

- the standard SPICE Gummel-Poon [2] *vertical* p-n-p model;
- subcircuits incorporating three SPICE Gummel-Poon models (representing one lateral p-n-p and two parasitic vertical p-n-p's) providing a prediction of substrate effects;
- in-house hybrid models adapted from one-dimensional vertical n-p-n formulations.

Because these models are often inaccurate, the use of lateral p-n-p transistors has been somewhat hampered since they cannot be accurately represented in a simulation environment. Furthermore, because these models neglect the complex two-dimensional (2D) nature of the lateral p-n-p, they are semi-empirical in nature and therefore lack the superiority of a truly physics-based formulation. As well as being more accurate than semi-empirical models, physics-based formulations possess the following advantages:

- model parameters have a physical significance leading to easier, more reliable parameter determination;
- to derive geometrical scaling rules;

- to assess the influence of process variations on device behavior,
- to facilitate realistic statistical modeling by physical correlation between model parameters.

This does not mean that all parameters are purely physical: for the depletion capacitances, e.g., the standard semi-empirical formula is used.

In this paper, we present a new compact model, called MODELLA, for the lateral p-n-p (oxide or junction-isolated) which is largely based on device physics. The basic modeling principles, the derivation of the main currents and charges, and the equivalent circuit topology are given in Section II. Model-specific aspects of parameter determination are discussed in Section III and this is followed in Section IV by results and discussion of comparisons between MODELLA and SPICE Gummel-Poon (GP) using measured device characteristics. Conclusions are given in Section V. A fully worked-out scheme for geometrical scaling rules, process dependence, and statistical modeling is beyond the scope of this present paper.

II. MODEL DERIVATION

In the derivation of MODELLA's analytical equations and equivalent circuit, the following modeling principles are used:

- basic model equations can be obtained from 1D analyses;
- 2D aspects of lateral p-n-p physics can then be incorporated by modifying these basic equations and the equivalent circuit to include the effects of series resistances, most notably current crowding.

Here 1D analyses refer to a 1D lateral p-n-p (obtained by taking a horizontal cross section just below the surface of the device shown in Fig. 1) and a 1D parasitic vertical p-n-p (obtained by taking a vertical cross section through the emitter contact on the left-hand side of the device shown in Fig. 1). The use of 1D formulations to model lateral p-n-p physics was shown to be valid by comparing these analytical predictions with the results of 2D numerical device simulations. By selectively increasing the majority-carrier mobility to very high values, it was possible to eliminate ohmic voltage drops in the simulations, thereby facilitating such a comparison. These comparisons proved, for example, that the collector current flow pattern exhibited no significant 2D high-injection effects, implying that the main 2D hole current density between emitter and collector could be accurately described at *all* injection levels by multiplying the hole current density of the 1D lateral p-n-p device. The multiplier from the 1D case to the 2D case depends on the device geometry, but not on the current level.

In the next few sections, a detailed derivation of MODELLA's main currents and charges for the forward active case will be presented, with the reverse active case following from symmetry. When applicable, these derivations will reflect the two modeling principles just out-

lined, i.e., a 1D derivation followed by a modification to incorporate 2D ohmic effects.

A. Collector Current and Early Effect

For lateral p-n-p compact modeling, we have adopted a physical approach to modeling the injection in the quasi-neutral epitaxial base region. The collector current I_c is related directly to the bias-dependent minority-carrier concentration $p(x)$, in the epitaxial base region of the 1D lateral p-n-p (c.f. [3], [4]). Because the hole distribution varies almost linearly with distance at *all* injection levels [5], we can assume that $p(x)$ varies linearly from a maximum value of p_e (a function of the emitter base voltage V_{eb}) at $x = 0$ near the emitter-base junction to a value zero at $x = X_b$ near the collector-base junction. X_b is the width of the neutral base region. Furthermore, we assume that a suitable average value for $p(x)$ in such a distribution is $p_e/2$ so that our effective hole diffusion coefficient D_p is defined in the center of the base region. Assuming a constant base doping (N_{epi}), quasi-neutrality ($n = p + N_{epi}$) and no recombination ($J_n = 0$ and hence $F = V_i \cdot n^{-1} \cdot dn/dx$), we can derive that [6]

$$\begin{aligned} J_p &= -qD_p \frac{2p + N_{epi}}{p + N_{epi}} \frac{dp}{dx} \\ &\approx qD_p \frac{p_e + N_{epi}}{p_e/2 + N_{epi}} \frac{p_e}{X_b} \end{aligned} \quad (1)$$

The minority-carrier concentration follows from the pn product at $x = 0$

$$p_e(p_e + N_{epi}) = n_i^2 \exp(V_{eb}/V_i)$$

or

$$\frac{p_e}{N_{epi}} = \frac{1}{2} \left\{ \sqrt{1 + 4 \left(\frac{n_i}{N_{epi}} \right)^2 \exp(V_{eb}/V_i)} - 1 \right\}. \quad (2)$$

Some manipulation then leads to an expression suitable for compact modeling

$$\begin{aligned} I'_c &= \frac{4I_f}{3 + \sqrt{1 + 16 \frac{I_f}{I_k}}} \\ I_f &= I_{sat} \{ \exp(V_{eb}/V_i) - 1 \} \\ I_{sat} &= \frac{q \cdot D_p \cdot n_i^2}{N_{epi} \cdot X_b} \cdot A_{eff} \\ I_k &= \frac{4 \cdot q \cdot D_p \cdot N_{epi}}{X_b} \cdot A_{eff} \end{aligned} \quad (3)$$

A_{eff} is the effective emitter area, V_i is the thermal voltage, and the two model parameters I_k and I_{sat} represent the high injection knee current and the saturation current, respectively [6]. Compared to the exact solution [7] of the differential equation in (1), the maximum deviation of (3) is

only 4%. This is in contrast to a maximum deviation of 15% with the expression of Chou [8] (who chose p_e as the average hole concentration instead of $p_e/2$) and a maximum deviation of 13% with the Gummel-Poon expression [9].

The Early effect [10] is modeled by including the effect of the collector-base depletion width X_{cb} , on the base width X_b between the metallurgical junctions of the emitter and collector, in the expression for the collector current

$$I_c = I'_c \cdot \frac{X_b}{X_{bj} - X_{cb}} = I'_c \cdot \frac{X_b}{X_b + X_{c0} - X_{cb}} \quad (4)$$

Here I'_c is the collector current without the Early effect (3) and X_{cb} is obtained by assuming asymmetric, abrupt, homogeneously doped junctions: $X_{cb} = X_{c0} \sqrt{1 - V_{cb}/V_d}$. In this way, we obtain a new expression modeling accurately both the high injection and forward Early effects in a homogeneously doped base transistor ($X_{c0} \ll X_b$)

$$I_c = \frac{I'_c}{1 - \sqrt{1 - \frac{V_{cb}}{V_d} / \left(1 + \frac{V_{eaf0}}{2V_d}\right)}} \quad (5)$$

where V_d and V_{cb} are the diffusion and collector-base voltages, respectively. In this equation the Early voltage at zero collector-base bias

$$V_{eaf0} = I_c \left/ \frac{dI_c}{dV_{cb}} \right|_{V_{cb}=0} = 2 \cdot V_d \cdot (X_b/X_{c0} - 1)$$

is the model parameter. By including the effect of the emitter-base depletion on the base width, this equation may be extended further, using one extra parameter V_{ear0} , to model the reverse Early effect.

An additional advantage of (5) is that punchthrough occurs at more physical values of V_{cb} . The approximate value of V_{cb} at which $X_{cb} = X_b$ is given by $V_{cb} \approx -V_{eaf0}^2/(4V_d)$ which is usually well above the avalanche breakdown voltage with open base BV_{ce0} . In the conventional modeling of the Early effect ($I_c = I'_c/(1 + V_{cb}/V_{eaf})$), punchthrough occurs at very low values of V_{cb} (i.e., $V_{cb} = -V_{eaf}$), which leads to numerical problems.

The modeling of 2D effects such as current crowding is based on the influence of the series resistances shown in Fig. 1. This figure shows how the hole current flow lines that make up the collector current, can be roughly divided into two distinct components: a purely lateral flow which originates at the emitter sidewall and a flow along curved trajectories which originates from the bottom of the emitter. At low current levels, the sidewall component dominates. At high current levels (not necessarily high injection), the voltage drop across the lateral emitter resistance $R_{e,at}$ leads to a debiasing of the sidewall junction thereby reducing the contribution from this component. The second component then dominates and current

crowding in the region under the emitter contact is observed. Numerical device simulations on 2D structures show that the larger effective base width associated with these trajectories has important consequences for device behavior at high current levels. The collector current and therefore the current gain H_{fe} can decrease by more than a factor of two and the Early effect is significantly reduced. This reduction in the Early effect is in agreement with the experimentally observed dependence of the Early voltage on the emitter-base voltage V_{eb} (see, for example, Fig. 5). It is crucial, therefore, to incorporate current crowding into a lateral p-n-p compact model and in MODELLE we do this by using double-emitter diodes and current sources to represent the sidewall ($I_{f,at}$) and bottom ($I_{f,ver}$) components of I_c . This separation of sidewall and bottom components of I_c can be seen in MODELLE's equivalent circuit shown in Fig. 2. $I_{f,at}$ and $I_{f,ver}$ are described by means of (3) and (5), but for the emitter-base voltage they use the internal junction voltages V_{e1b} and V_{e2b1} , respectively, and for the collector voltage V_{c1b} . In addition, different saturation current and Early voltage parameters are used in the respective expressions, reflecting the different effective basewidths associated with the two current paths. The saturation current I_{sat} is divided between $I_{f,at}$ and $I_{f,ver}$ by introducing a parameter $XIFV$ which represents the fraction of the collector current originating from under the emitter (typically 10–20%). Equation (3) is premultiplied by $(1 - XIFV)$ to obtain $I_{f,at}$ and by $XIFV$ to obtain $I_{f,ver}$. At low current levels, when $V_{e1b} \approx V_{e2b1}$, $I_{f,at}$ dominates due to its larger saturation current, whereas at high current levels $I_{f,ver}$ takes over due to the voltage drop across $R_{e,at}$. The Early voltage parameter associated with $I_{f,ver}$ (i.e., V_{eaf0v}) will be larger than that used with $I_{f,at}$ (i.e., V_{eaf0l}), thus modeling the dependence of the Early voltage on V_{eb} . At low forward bias, the Early voltage, V_{eaf} , at $V_{cb} = 0$ will be approximately equal to V_{eaf0l} , whereas at high forward bias V_{eaf} will be significantly larger and will depend on V_{eaf0v} .

B. Base Current

The ideal base current I_{RE} mainly originates from electrons injected into the emitter which recombine at the emitter contact. Because these minority carriers are injected from the epilayer base region under the emitter contact, the diode I_{RE} is located between nodes e_2 and b_1 in the equivalent circuit. Similarly, the nonideal base current I_{LE} depends on V_{e2b1} because it mainly originates from space-charge recombination under the emitter due to the large ratio of bottom-to-sidewall areas. The equation used for I_{LE} is derived from the standard Shockley-Read-Hall formulation and is described in [6]. In certain processes other origins of base current may become relatively significant (Si-SiO₂ interface recombination with poor oxide quality and bulk recombination with double-poly processes), but except for extreme circumstances, they retain the ideal and nonideal behavior of I_{RE} and I_{LE} and thus can be adequately modeled.

other compact models [6]; the current dependence is not included, but the internal voltage drop is.

E. Summary

MODELLE has 42 parameters and 6 internal nodes which make it more complex than the SPICE GP model. However, due to the symmetry of its equivalent circuit, which reflects the symmetry in the physical structure of the lateral p-n-p, and due to the explicit nature of its equations, MODELLE's equivalent circuit is quite straightforward to solve, requiring no additional iterative procedures. The symmetry referred to here also applies to the equations and parameters used in the reverse active case. MODELLE therefore provides reverse active modeling with the same level of accuracy as the forward active case.

The modeling of current crowding has led to the separation of the sidewall and bottom parts of the emitter-base and collector-base junctions. This has the beneficial effect that the *location* of elements in the equivalent circuit can reflect the location of the underlying physical mechanisms in actual devices. The emitter-base depletion charge Q_{ET} , for example, is located in a more physical way under the emitter rather than at the sidewall.

III. PARAMETER DETERMINATION

The strategy chosen for the determination of the 42 MODELLE parameters is based on the least squares optimization of parameters from measured device characteristics, augmented by the calculation of a small number of parameters from process information. Because MODELLE is a physical model, all parameters are closely related to and can be expressed in terms of the underlying physics. This greatly enhances the reliability of calculated values for parameters and the physical plausibility of optimized parameter values can be verified. In this section, we discuss some key points in the strategy which are of a model-specific nature. Again the forward active case will be discussed, with the reverse active parameter determination following from symmetry. Although in this paper measured data are used for parameter extraction, similar results can be obtained by using computer device simulations as input for the parameter extraction.

A. The Ning-Tang Method

In MODELLE the base resistance R_{be} consists of a constant part R_{bec} and a conductivity modulated part R_{bv} . The low injection value of R_{bv} is easily calculated from a knowledge of the epilayer resistivity and geometrical considerations. Now, R_{bec} and the emitter contact resistance R_{ex} can be optimized by fitting the emitter current I_e at high forward bias. However, this method is undesirable because a prerequisite is a perfect model prediction of the fall off in the current gain H_{fe} .

The method of Ning and Tang [12] measures the voltage deviation δV of I_b from the ideal I_b versus V_{eb} characteristic at high current levels in order to extract emitter

and base resistance parameters. For the lateral p-n-p we can write

$$\delta V = I_e R_e + I_b R_{be} \quad (10)$$

where

$$I_e = I_c + I_b + I_{sub}$$

$$R_e = R_{ex}$$

$$R_{be} = R_{bec} + R_{bv}$$

Therefore

$$\frac{\delta V}{I_c} = R_{ex} \left(1 + \frac{I_{sub}}{I_c} \right) + \frac{R_{bv}}{H_{fe}} + \frac{R_{ex} + R_{bec}}{H_{fe}} \quad (11)$$

Normally $I_{sub}/I_c \ll 1$ and therefore it may be neglected.

If we make the assumption that R_{bv}/H_{fe} is constant at all injection levels, then a plot of $\delta V/I_c$ versus H_{fe}^{-1} yields a straight line (see Fig. 3) which has as its slope $R_{ex} + R_{bec}$ and as its extrapolated y-axis intercept $R_{ex} + R_{bv}/H_{fe}$. Because we have already calculated R_{bv} at low injection, we can easily determine R_{ex} and R_{bec} using this curve.

The correct interpretation of the curve is dependent on the validity of the assumption that R_{bv}/H_{fe} is constant. This assumption is rarely valid in vertical n-p-n transistors for the following reasons.

1) Current crowding at the emitter-base sidewall is usually present. This leads to a dramatic reduction in R_{bv} , but has relatively little influence on H_{fe} .

2) The influence of quasi-saturation on H_{fe} increases the ratio.

Because of these effects and the difficulty in quantifying them, the interpretation of the curve is often rather dubious in the case of the vertical n-p-n transistor. With the lateral p-n-p these points can be effectively circumvented so that only high injection of the homogeneously doped base region in the lateral p-n-p remains. This has the desired effect of maintaining an approximately constant ratio between R_{bv} and H_{fe} because it lowers both H_{fe} and R_{bv} by means of charge storage and conductivity modulation.

The conclusion is that the method of Ning and Tang is highly suitable for the lateral p-n-p, the only prerequisite being that the condition $I_{sub}/I_c \ll 1$ be satisfied. In practice this method has yielded remarkably consistent results in the determination of R_{ex} and R_{bec} . The accuracy, however, is influenced by the calculation of R_{bv} .

B. The Early Parameters

The optimization of the forward Early parameters V_{eaf0_1} and V_{eaf0_2} , associated with $I_{f_{lat}}$ and $I_{f_{ver}}$, respectively, proved to be quite problematic. This was because a realistic optimization of V_{eaf0_1} , required a high forward emitter-base bias in order to induce current crowding under the emitter whereby $I_{f_{ver}}$ constituted most of the collector current. The usual approach of optimizing the Early parameters to fit I_c as a function of reverse collector-base

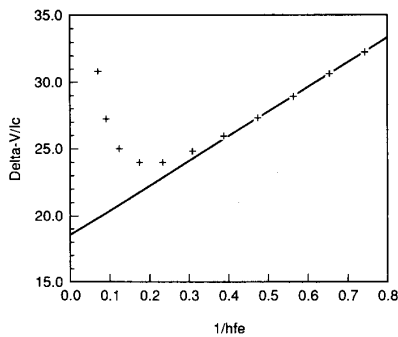


Fig. 3. Characteristic curve obtained using the method of Ning and Tang. The straight line extrapolation is indicated.

bias at constant V_{eb} was unreliable because of the following factors:

1) At high current levels, the Early voltage V_{eaf} , defined as

$$V_{eaf} = I_c \left/ \frac{dV_{cb}}{dI_c} \right|_{V_{eb} = \text{constant}}$$

is overestimated due to ohmic voltage drop across R_{ex} which compensates the increase in I_c due to V_{cb} variation.

2) Incorrect interpretation of the Early effect as a result of internal heating caused by dissipation. At constant V_{eb} the temperature rise will cause a large increase in I_c because of the temperature dependence of the collector saturation current I_{sat} .

By defining the Early voltage at constant base current, i.e.,

$$V_{eaf} = I_c \left/ \frac{dV_{cb}}{dI_c} \right|_{I_b = \text{constant}}$$

the first problem is eliminated and the second problem is drastically reduced since the temperature dependence of the forward current gain H_{fe} is much less than that of I_{sat} . Using the nonsaturation region of the I_c versus V_{ec} characteristic to optimize the Early parameters therefore allowed us to determine reliable values for the Early parameters at low and high forward bias.

C. Charge Parameters

The two low-injection transit time parameters $\tau_{f\text{lat}}$ and $\tau_{f\text{ver}}$, associated with $Q_{f\text{lat}}$ and $Q_{f\text{ver}}$, respectively, were optimized together by fitting the cutoff frequency f_T versus I_c characteristic. Since these charges have quite different sensitivities to V_{cb} ($Q_{f\text{ver}}$ is not affected by V_{cb} , but $Q_{f\text{lat}}$ is, see Section II-D), the reliability of these optimizations was greatly enhanced by simultaneously fitting two or more f_T characteristics having different V_{cb} values.

D. High Injection and Current Crowding Parameters

The seemingly intractable problem of separating the effects of high injection and current crowding from measured device characteristics was solved using a somewhat

heuristic approach. An advantage of using a physics-based approach to model high injection in the lateral p-n-p is that only one parameter I_k is required to indicate the onset of high injection in I_c and I_{sub} (forward active) and also in I_e and I_{sub} (reverse active). See also (3) and (6). Therefore, the value of I_k , obtained by fitting, say, the initial fall-off in the forward current gain characteristic, could be checked to ensure compatibility with the reverse current gain characteristic or the forward and reverse I_{sub}/I_b characteristics. In this way, a quite reliable value for I_k is always obtained. Once a value for I_k is established the current crowding parameters $XIFV$ and $R_{e\text{lat}}$ are then optimized by fitting the remaining fall-off in the H_{fe} characteristic at high forward bias. A good initial guess for $XIFV$ can be provided by analytical expressions derived from approximating the 2D hole current trajectory pattern in the epitaxial base region by quarter circles and straight-line segments. With this approximation the saturation current per unit stripe length for $I_{f\text{ver}}$ becomes [8], [14]

$$I_{sv} = \frac{q \cdot D_p \cdot n_i^2}{\pi \cdot N_{\text{epi}}} \cdot \ln \left(1 + \pi \frac{Y_{\text{cpi}} - Y_e}{X_b} \right). \quad (12)$$

For the lateral current we have (see also Fig. 1)

$$I_{sl} = \frac{q \cdot D_p \cdot n_i^2}{N_{\text{epi}} \cdot X_b} \cdot Y_e. \quad (13)$$

So $XIFV$ can be calculated from $XIFV = I_{sv}/(I_{sv} + I_{sl})$. For the example in Section IV we find then $XIFV = 0.43$, which is close to the value found from optimization (0.5). Because of the sensitivity of the Early voltage, V_{eaf} , as a function of V_{cb} to current crowding (see Section II-A), curves of V_{eaf} versus V_{eb} provide a qualitative verification of the plausibility of $XIFV$ and $R_{e\text{lat}}$ values.

Our experience has shown that an almost totally automated parameter determination strategy for MODELLEA can be used with the vast majority of devices. In cases, though, where problems arise, the type of heuristic methods outlined above yield a solution which only a physics-based compact model can provide.

IV. RESULTS AND DISCUSSION

In order to illustrate some important aspects of MODELLEA's performance, a comparison was made between MODELLEA and the SPICE GP p-n-p model [2]. The SPICE GP model was chosen because it is probably the most widely used compact model, either on a stand-alone basis or as part of a subcircuit. Since SPICE GP does not model substrate effects, the reader is referred to [9], [13] for a comparison between MODELLEA and an extended GP model which does contain substrate effects.

The device chosen for comparison purposes is a typical junction-isolated lateral p-n-p where the mask base width $X_b = 4 \mu\text{m}$ ($3 \mu\text{m}$ in silicon) and the collector completely surrounds the square $8 \times 8 \mu\text{m}^2$ emitter. The junction depth of both emitter and collector $Y_e = 0.7 \mu\text{m}$, the epitaxial base doping concentration is $3.5 \times 10^{15} \text{ cm}^{-3}$ and $Y_{\text{cpi}} = 1.4 \mu\text{m}$ (see Fig. 1). The forward Gummel plot

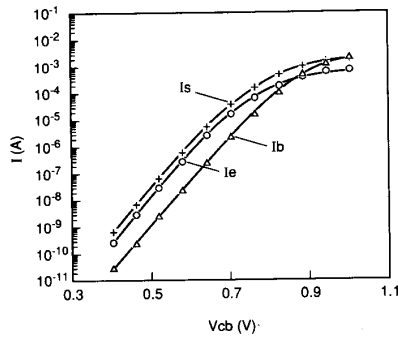


Fig. 4. Reverse active Gummel plot of the junction isolated device. The solid lines represent MODELLEA and the points are measured data: \times —substrate current; \circ —emitter current, \triangle —base current.

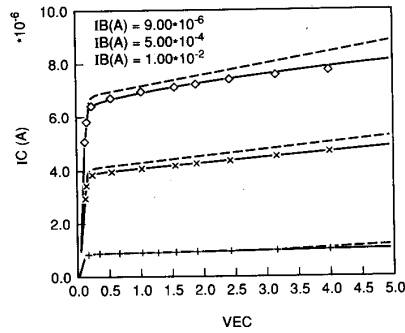


Fig. 5. I_c versus V_{ec} characteristic at three different values of base current. The solid lines represent MODELLEA, the dashed lines the SPICE GP model, and the points are measured values.

is not shown as both models provided good agreement with measured data (the SPICE GP model provided no prediction of the substrate current though). Again, the reverse Gummel plot showed no major difference in model predictions of I_e and I_b . However, Fig. 4 shows that the substrate current is now the largest current, and MODELLEA predicts very well. In Fig. 5 MODELLEA provides a much better prediction of the saturation region of the I_c versus V_{ec} characteristic due to its improved resistive network and the reverse I_{sub} modeling.

With the GP model the Early voltage, V_{eaf} , has a negligible dependence on V_{cb} and as shown in Fig. 6 is completely independent of V_{cb} . MODELLEA, on the other hand, shows excellent agreement with measured data due to the physical modeling of both basewidth modulation by V_{cb} and current crowding under the emitter. This bias dependence of V_{eaf} is often a critical aspect in lateral p-n-p compact modeling, e.g., in circuit applications involving lateral p-n-p current sources.

The improved modeling of the f_T characteristic by MODELLEA in Fig. 7 is due to a) the inclusion of the Webster effect, b) the fact that the f_T fall-off at high current levels in MODELLEA is a function not only of high injection, but also of current crowding, and c) the way in which the stored base charge is divided into two components with differing V_{cb} dependencies. An inconsistent SPICE GP charge model, in which the substrate is connected to the

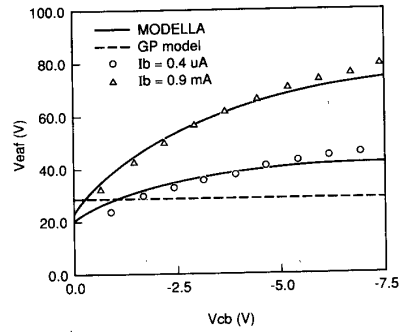


Fig. 6. Comparison between MODELLEA and SPICE GP predictions of the measured Early voltage, V_{eaf} , as a function of V_{cb} . The Early voltage is defined as

$$V_{eaf} = I_c \left. \frac{dV_{cb}}{dI_c} \right|_{I_b = \text{constant}} - V_{cb}$$

The two I_b values correspond to $V_{eb} = 0.7$ V and $V_{eb} = 0.94$ V, respectively.

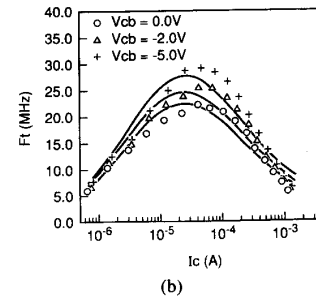
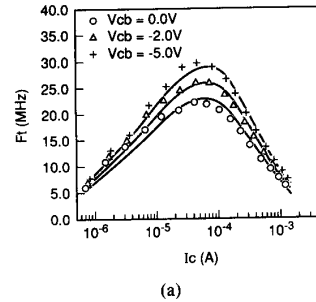


Fig. 7. Comparison between (a) MODELLEA and (b) SPICE GP model predictions of the measured cutoff frequency f_T as a function of I_c at different V_{cb} values.

collector, leads to even greater differences in the two f_T characteristics.

Finally, a comparison between the H_{fe} predictions of MODELLEA and SPICE GP is shown for another junction-isolated device which exhibited a high-temperature effect. The generation current of the reverse-biased substrate-base junction can become large enough with increasing temperature to compensate the terminal base current. In this situation, the current gain increases dramatically in the low forward-bias region. A set of physical temperature scaling rules has been derived for MODELLEA's parameters and Fig. 8 shows how the temperature-scaled

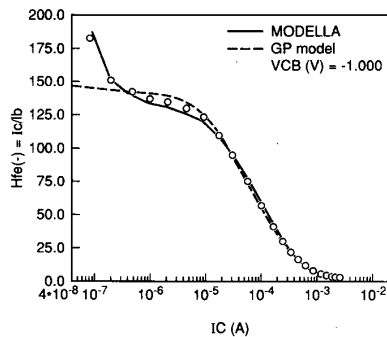


Fig. 8. Comparison between MODELLA and SPICE GP model predictions of the measured current gain H_{fe} at 120°C of a junction-isolated device. The points are measured data, the dashed line SPICE GP, and the solid line MODELLA.

generation parameter of the substrate-base diode I_{sf} predicts this compensation effect.

With regard to the circuit simulation environment, extensive test simulations have shown that MODELLA exhibits excellent convergence behavior on a par with the SPICE GP model. In terms of C.P.U. time, MODELLA is a factor of 1.5–2.0 slower than the SPICE GP model while the number of iterations required for convergence is roughly equal.

V. CONCLUSIONS

This paper describes the first truly physics-based lateral p-n-p compact model incorporating high injection effects, current crowding effects, and a bias-dependent output conductance. MODELLA's performance is significantly better than the SPICE GP model especially with respect to reverse active and saturation modeling, and the bias dependencies of the cutoff frequency and the Early voltage. The physical significance of MODELLA's parameters leads to easier and more reliable parameter determination. Furthermore, the realistic incorporation of a lateral p-n-p compact model into integrated systems, linking process, device, and circuit simulation, should now be possible.

ACKNOWLEDGMENT

The authors wish to thank M. Koolen, H. Geelen, and H. Timmerman for providing the lateral p-n-p measurements.

REFERENCES

- [1] I. Kidron, "Integrated circuit model for lateral pnp transistors including isolation junction interaction," *Int. J. Electron.*, vol. 31, p. 421, 1971.
- [2] A. Vladimirescu et al., *Spice version 2G.5 User's Guide*. Berkeley, CA: Berkeley Univ., 1981.
- [3] F. G. O'Hara, "Physically based compact modelling of lateral pnp transistors," M.Sc. thesis, Trinity College Dublin, Dublin, Ireland, 1990.
- [4] H. C. de Graaff and W. J. Kloosterman, "New formulation of the current and charge relations in bipolar transistor modelling for CAD

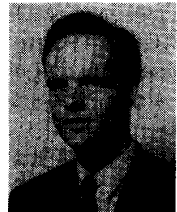
purposes," *IEEE Trans. Electron Devices*, vol. ED-32, no. 11, Nov. 1985.

- [5] J. Lindmayer and C. Y. Wrigley, *Fundamentals of Semiconductor Devices*. Princeton, NJ: Van Nostrand, 1965.
- [6] H. C. de Graaff and F. M. Klaassen, *Compact Transistor Modelling for Circuit Design*. New York: Springer-Verlag, 1990, ch. 3.
- [7] A. van der Ziel, *Solid State Physical Electronics*. Englewood Cliffs, NJ: Prentice-Hall, 1968, eq. 16.71.
- [8] S. Chou, "An investigation of lateral transistors—DC characteristics," *Solid-State Electron.*, vol. 14, p. 811, 1971.
- [9] H. C. de Graaff and F. M. Klaassen, *Compact Transistor Modeling for Circuit Design*. New York: Springer-Verlag, 1990, ch. 5.
- [10] J. M. Early, "Effects of space-charge widening in junction transistors," *Proc. IRE*, vol. 40, p. 1401, 1952.
- [11] W. M. Webster, vol. *Proc. IRE*, vol. 42, p. 914, 1954.
- [12] T. H. Ning and D. D. Tang, "Method for determining the emitter and base series resistances of bipolar transistors," *IEEE Trans. Electron Devices*, vol. ED-31, p. 409, 1984.
- [13] F. G. O'Hara, J. J. H. van den Biesen, H. C. de Graaff, and J. B. Foley, "A new physical compact model for lateral pnp transistors," in *Proc. IEEE, Bipolar Circuits and Technology Meet.* (Minneapolis, MN), Sept. 1990, p. 102.
- [14] K. S. Seo and C. K. Kim, "On the geometrical factor of lateral p-n-p transistors," *IEEE Trans. Electron Devices*, vol. ED-27, p. 295, Jan. 1980.



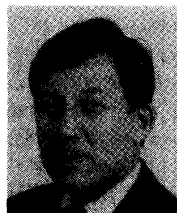
Francis G. O'Hara received the B.E. degree in electronic engineering from University College Dublin, Ireland, in 1985 and the M.Sc. degree by research in electronic engineering from Trinity College Dublin, Ireland, in 1990.

In 1985 he joined Philips Research Laboratories in Eindhoven, The Netherlands, where he worked on numerical device simulation and the physics and compact modelling of bipolar devices. While at Philips he also undertook study towards the M.Sc. degree by research in electronic engineering. In 1991 he emigrated to Australia and now works for Teletronics Pacing Systems, Sydney, where he is an implant software team leader on an implantable cardiac defibrillator project. His interests now include real-time software for embedded control systems and cardiac physiology.



Jan J. H. van den Biesen received the M.S. and Ph.D. degrees in physics from the University of Leiden, Leiden, The Netherlands, in 1977 and 1982, respectively.

After a year of additional research on molecular beam scattering at the Lawrence Berkeley Laboratory in Berkeley, CA, he joined the Philips Research Laboratories in Eindhoven, The Netherlands, in 1983, where he became involved in the modeling of bipolar transistors. From 1986 to 1987 he worked at the Central Research Laboratory of Hitachi, Ltd., in Tokyo as an exchange researcher. Soon after his return to Eindhoven, he moved to the Management Office of the Philips Research Laboratories. Currently, he is engaged in government relations.



H. C. de Graaff was born in Rotterdam, The Netherlands, in 1933. He received the M.S. degree in electrical engineering from the Delft University of Technology, Delft, The Netherlands, in 1956, and the Ph.D. degree from the Eindhoven University of Technology, Eindhoven, The Netherlands, in 1975.

He joined Philips Research Laboratories, Eindhoven, in 1964, and has been working on thin-film transistors, MOST, bipolar devices, and materials research on polycrystalline silicon. His present

field of interest is device modeling for circuit simulation. Since his retirement from Philips Research (November 1991) he has been a consultant to the University of Twente and the Technical University of Delft, both in The Netherlands.



W. J. Kloosterman was born in Olst, The Netherlands, in July 1951. He graduated from the Technical College in Zwolle in 1974.

He joined Philips Research Laboratories, Eindhoven, The Netherlands, in 1974. First he worked on finite-element methods in mechanical engineering, and, since 1980, has been involved in CACD, transistor modeling, and parameter extraction.



J. Brian Foley (M'89) was born in Dublin, Ireland, on December 24, 1949. He received the B.E. (elec.) degree in 1972 from the National University of Ireland (University College Dublin) and the M.E.E. degree in 1974 from the Philips International Institute/Technical University, Eindhoven, The Netherlands. He obtained the Ph.D. degree from the University of Dublin in 1988 for a thesis on noise canceling adaptive filters.

From 1974 to 1980 he lectured at the College of Technology, Kevin St., Dublin, on digital and analog circuit design. Since 1980, he has been with the Department of Microelectronics and Electrical Engineering at the University of Dublin (Trinity College), where he has been responsible for courses and research projects in integrated circuit design, with particular emphasis on digital signal processing elements and high-speed circuit performance. He is also involved in research in adaptive signal processing for acoustic echo cancellation.